Preprint typeset in JHEP style - HYPER VERSION

CERN-PH-TH/2008-118
CP3-08-12
DCPT/08/80
IPPP/08/40
MCnet/08/02



# A Positive-Weight Next-to-Leading Order Monte Carlo Simulation of Drell-Yan Vector Boson Production

**Keith Hamilton**

*Centre for Particle Physics and Phenomenology (CP3),*
*Université Catholique de Louvain,*
*Chemin du Cyclotron 2, 1348 Louvain-la-Neuve, Belgium.*
*Email:* keith.hamilton@uclouvain.be

**Peter Richardson**

*Institute of Particle Physics Phenomenology, Department of Physics,*
*University of Durham, Durham, DH1 3LE, UK; and*
*Theoretical Physics Group, CERN, CH-1211 Geneva 23, Switzerland.*
*Email:* peter.richardson@durham.ac.uk

**Jon Tully**

*Institute of Particle Physics Phenomenology, Department of Physics,*
*University of Durham, Durham, DH1 3LE, UK.*
*Email:* j.m.tully@durham.ac.uk

Abstract: The positive weight next-to-leading-order (NLO) matching scheme (POWHEG) is applied to Drell-Yan vector boson production in the Herwig++ Monte Carlo event generator. This approach consistently combines the NLO calculation and parton shower simulation, without the production of negative weight events. The simulation includes a full implementation of the truncated shower required to correctly describe soft emissions in an angular-ordered parton shower, for the first time. The results are compared with Tevatron $W^{\pm}$ and $Z$ production data and predictions for the transverse momentum spectrum of gauge bosons at the LHC presented.

Keywords: QCD, Phenomenological Models, Hadronic Colliders.

## Contents



## 1. Introduction

Monte Carlo simulations traditionally combine leading-order $2 \to 2$ matrix elements with parton showers which provide resummation of soft and collinear radiation. This provides a fully exclusive description of observables which allows evolution to the hadronization scale where models of the non-perturbative regime can be incorporated. This makes Monte Carlo simulations an essential tool in experimental analysis allowing a fully exclusive description of the final state to be compared directly with experimental results.

Parton shower simulations include the leading-logarithmically, and an important subset of the next-to-leading-logarithmically, enhanced contributions and therefore underestimate the radiation of high transverse momentum ($p_T$) partons. The Monte Carlo description can be improved by matching to higher-order matrix elements which correctly describe the production of high $p_T$ particles. A number of approaches have been developed to correct the emission of the hardest parton in an event. In the PYTHIA event generator [1], corrections were included for $e^+e^-$ annihilation [2], deep inelastic scattering [3], heavy particle decays [4] and vector boson production in hadron collisions [5]. In the HERWIG event generator [6,7] corrections were included for $e^+e^-$ annihilation [8], deep inelastic scattering [9],

top quark decays [10] and vector boson production [11] in hadron-hadron collisions following the general method described in [12, 13].[1] These corrections had to be calculated for each individual process and only corrected the first or hardest[2] emission, in addition the method can only be applied to relatively simple cases and the leading-order normalisation of the cross section is retained.

In recent years there have been a number of additional developments which aim to improve on these results by either providing a description of the hardest emission together with a next-to-leading order (NLO) cross section [19–31],[3] or the emission of more than one hard parton at leading order [32–37].[4] These matching prescriptions are complicated because the regions of phase space filled by the higher-order matrix elements and the parton shower must be smoothly separated in order to avoid problems such as double-counting, where the shower and matrix elements radiate in the same region. In general the major complication is gaining an analytic understanding of the result of the parton shower either, to subtract it from the real emission matrix element, as in the MC@NLO approach [19–24], or to reweight the real emission matrix elements so they can be merged with the parton shower in multi-parton matching.

The first successful scheme for matching at NLO was the MC@NLO approach [19–24] which has been implemented with the HERWIG event generator for many processes. The method has two draw backs; first, it involves the addition of correction terms that are not positive definite and therefore can result in events with a negative weight and second, the implementation of the method is heavily dependent on the details of the parton shower algorithm used by the event generator.

In Ref. [26] a novel method, referred to as POWHEG (POsitive Weight Hardest Emission Generator), was introduced to achieve the same aims as MC@NLO while creating only positive weight events and being independent of the event generator with which it is implemented. The POWHEG method has been applied to $Z$ pair hadroproduction [27], heavy flavour hadroproduction [30] and $e^+e^-$ annihilation to hadrons [31]. A general outline of the ingredients required for POWHEG with two popular NLO subtraction schemes is given in Ref. [29].

The POWHEG shower algorithm involves generating the hardest emission in $p_T$ separately using a Sudakov form factor containing the full matrix element for the emission of an extra parton and adding to this vetoed showers, which produces radiation at lower scales in the shower evolution variable, and a truncated shower, which generates radiation at higher scales in the shower evolution variable, than the scale of the highest $p_T$ emission. While the POWHEG scheme is independent of the parton shower algorithm, it does require the parton shower to be able to produce vetoed and truncated showers. The ability to perform vetoed

[1] Herwig++ includes matrix element corrections for $e^+e^-$ annihilation [14], top quark decays [15], vector boson production [16] in hadron-hadron collisions and Higgs production in gluon fusion [17] using the approach of Refs. [12, 13] and the improved angular-ordered parton shower of Ref. [18].

[2] In PYTHIA the first emission was corrected whereas in HERWIG any emission which could be the hardest was corrected.

[3] There have been other theoretical ideas but only the MC@NLO and POWHEG methods have led to practical programs whose results can be compared with experimental data.

[4] A recent comparison of these approaches can be found in [38].

showers is present in most modern Monte Carlo event generators, however some changes are required to enable them to generate truncated showers. Although the POWHEG approach is formally correct to the same accuracy as the MC@NLO technique the two methods differ in their treatment of sub-leading terms.

In this work the POWHEG approach is applied Drell-Yan vector boson production with the Herwig++ [17,39] event generator. A full truncated shower is implemented for the first time.[5]

The paper is organised as follows. In Sect. 2 we outline the main features of the POWHEG method. In Sect. 3 we collect the essential formulae relating to the NLO cross section, for implementation in the program. In Section 4 we give details of the event generation process for the hard configurations, this is followed by a description of how these configurations are subsequently reproduced by the Herwig++ angular-ordered parton shower, thereby accounting for colour coherence effects associated with soft wide angle parton emissions. In Sect. 5 we present the results of our implementation, comparing it to Tevatron data, and in Sect. 6 we give our conclusions.

## 2. The POWHEG method

In the POWHEG approach [26] the NLO differential cross section for a given $N$-body process can be written as

$$\mathrm{d}\sigma = \overline{B}\left(\Phi_B\right)\,\mathrm{d}\Phi_B\,\left[\Delta_{\hat{R}}\left(0\right) + \frac{\hat{R}\left(\Phi_B,\Phi_R\right)}{B\left(\Phi_B\right)}\,\Delta_{\hat{R}}\left(k_T\left(\Phi_B,\Phi_R\right)\right)\,\mathrm{d}\Phi_R\right], \tag{2.1}$$

where $\overline{B}\left(\Phi_B\right)$ is defined as

$$\overline{B}\left(\Phi_B\right) = B\left(\Phi_B\right) + V\left(\Phi_B\right) + \int \hat{R}\left(\Phi_B,\Phi_R\right) - \sum_i C_i\left(\Phi_B,\Phi_R\right)\,\mathrm{d}\Phi_R, \tag{2.2}$$

$B\left(\Phi_B\right)$ is the leading-order contribution, dependent on the $N$-body phase space variables $\Phi_B$, the *Born variables*. The regularized virtual term $V\left(\Phi_B\right)$ is a finite contribution arising from the combination of unresolvable, real emission and virtual loop contributions. The remaining terms in square brackets are due to $N$+1-body real emission processes which depend on both the Born variables and additional *radiative variables*, $\Phi_R$, parametrizing the emission of the extra parton. The real emission term, $\hat{R}\left(\Phi_B,\Phi_R\right)$, is given by a sum of parton flux factors multiplied by real emission matrix elements for each channel contributing to the NLO cross section. Finally, each term $C_i\left(\Phi_B,\Phi_R\right)$ corresponds to a combination of *real counterterms/counter-event weights*, regulating the singularities in $\hat{R}\left(\Phi_B,\Phi_R\right)$. The modified Sudakov form factor is defined as

$$\Delta_{\hat{R}}\left(p_T\right) = \exp\left[-\int \mathrm{d}\Phi_R\,\frac{\hat{R}\left(\Phi_B,\Phi_R\right)}{B\left(\Phi_B\right)}\,\theta\left(k_T\left(\Phi_B,\Phi_R\right) - p_T\right)\right], \tag{2.3}$$

[5] Truncated shower effects were neglected in Refs. [27, 30], while an approximate treatment was used in Ref. [31] where at most one truncated emission was generated.

where $k_T(\Phi_B, \Phi_R)$ is equal to the transverse momentum of the extra parton in the collinear and soft limits.

In the framework of a conventional parton shower Monte Carlo program the Sudakov form factor $\Delta_{\tilde{R}}(p_T)$ has the same form as that in Eq. 2.3 but with $\tilde{R}(\Phi_B, \Phi_R)$ replacing $\hat{R}(\Phi_B, \Phi_R)$, where the former is typically the sum of the real emission matrix elements approximated by their soft/collinear limits. This object has an interpretation as the *probability* that given some initial configuration of partons resolved at some characteristic scale $p_T^i$, in *evolving* to some other resolution scale, $p_T$, no further partons are resolved. The parton shower approximation to the NLO differential cross section is analogously given by

$$\mathrm{d}\tilde{\sigma} = B(\Phi_B)\,\mathrm{d}\Phi_B \left[\Delta_{\tilde{R}}(0) + \frac{\tilde{R}(\Phi_B, \Phi_R)}{B(\Phi_B)}\,\Delta_{\tilde{R}}(k_T(\Phi_B, \Phi_R))\,\mathrm{d}\Phi_R\right]. \tag{2.4}$$

The first term in Eq. 2.4 gives a differential distribution proportional to the leading-order differential cross section, which is retained in the absence of any parton showering, *i.e.* with probability $\Delta_{\tilde{R}}(0)$ (non-radiative events), while the second term represents the probability of evolving from the starting scale to scale $p_T$ at which point an emission is generated according to $\tilde{R}(\Phi_B, \Phi_R)\Big|_{p_T}$. The term in square brackets in Eqs. 2.1 and 2.4 is equal to unity when integrated over the radiative phase space.

In the POWHEG framework the parton shower is promoted to NLO accuracy by demanding that the non-radiative events are distributed according to the first term in Eq. 2.1 and that the hardest (highest $p_T$) emission is distributed according to the second term. Whereas in the conventional simulation an $N$-body configuration is generated according to $B(\Phi_B)$ and then showered using the Sudakov form factor $\Delta_{\tilde{R}}$, the POWHEG formalism requires that the $N$-body configuration is generated according to $\overline{B}(\Phi_B)$ and then showered with the modified Sudakov form factor $\Delta_{\hat{R}}$. As the $\overline{B}(\Phi_B)$ term is simply the NLO differential cross section integrated over the radiative variables, it is naturally positive, which is reflected in the absence of events with negative weights, which are an unpleasant feature of other next-to-leading order matching schemes.

Since any further emissions constitute higher-order terms in the differential cross section, next-to-next-to-leading order and beyond, we may generate higher multiplicities in the usual way, by showering the radiative events using the standard parton shower algorithm. These showers must not generate emissions with $p_T$ greater than that of the emitted parton in the event generated according to Eq. 2.1,[6] they must be *vetoed showers*. For a parton shower which evolves in $p_T$ the POWHEG implementation is a trivial task; one simply initiates a parton shower from each external leg of the radiative POWHEG event using its $p_T$ as the initial-evolution scale.

Angular-ordered parton showers account for the phenomenon of QCD coherence where wide-angle soft gluon emissions, from near collinear configurations of two or more partons, have insufficient transverse resolving power to be sensitive to the constituent emitters. In effect the resulting radiation pattern is determined by the colour charge and momentum

[6] Should the POWHEG event turn out to be a non-radiative event, the $p_T$ veto scale is zero so these events remain as no-emission events.

of the *mother* of the emitters, rather than the emitters themselves. Ordering branchings in the parton shower in terms of the angle between the branching products takes this logarithmically enhanced effect into account; wide-angle soft partons are emitted from the mother of any subsequent smaller angle splittings by construction.

As well as circumventing the problem of negative event weights, a second major success of the POWHEG method is in defining how the highest $p_T$ emission may be modified to include the logarithmically enhanced effects of this soft wide-angle radiation. In Ref. [26] it was shown how the angular-ordered parton shower which produces the hardest emission, may be decomposed into a *truncated shower* simulating coherent, soft wide-angle emissions, followed by the highest $p_T$ (hardest) emission, followed again by further *vetoed parton showers*, comprising of lower $p_T$, smaller angle emissions. Performing this decomposition established the form of the truncated and vetoed showers, thereby describing all of the ingredients necessary to shower the radiative events in the POWHEG approach. This procedure was proven in [29] to give agreement with the NLO cross section, for all inclusive observables, while retaining the logarithmic accuracy of the shower.

In the POWHEG framework positive weight events distributed with NLO accuracy can be showered to resum further logarithmically enhanced corrections by:

- generating an event according to Eq. 2.1;
- directly hadronizing non-radiative events;
- mapping the radiative variables parametrizing the emission into the evolution scale, momentum fraction and azimuthal angle ($\tilde{q}_h$, $z_h$, $\phi_h$), from which the parton shower would reconstruct identical momenta;
- using the original leading-order configuration from $\overline{B}(\Phi_B)$ evolve the leg emitting the extra radiation from the default initial scale down to $\tilde{q}_h$ using the truncated shower;
- inserting a branching with parameters ($\tilde{q}_h$, $z_h$, $\phi_h$) into the shower when the evolution scale reaches $\tilde{q}_h$;
- generating $p_T$ vetoed showers from all external legs.

This procedure allows the generation of the truncated shower for the first time with only a few changes to the normal Herwig++ shower algorithm.

## 3. Next-to-Leading Order Cross Section

Although the NLO cross section for the Drell-Yan process was calculated nearly 30 years ago [40,41], we have implemented an independent calculation of it more suited to our present goal, including the decay of the vector boson and $\gamma/Z$ interference effects. In this section we collect the ingredients that arise in the NLO calculation for $q + \bar{q} \to l + \bar{l}$, necessary to describe our implementation of the POWHEG method.

### 3.1 Kinematics and phase space

The leading-order process under study is of the type, $\bar{p}_\oplus + \bar{p}_\ominus \to \bar{p}_1 + ... + \bar{p}_N$, in which all particles in the $N$-body final state are colourless. We denote the incoming hadron momenta $P_{\circledast}$, for hadrons incident in the $\pm z$ directions, respectively. The corresponding massless parton momenta, with momentum fractions $\bar{x}_\oplus$ and $\bar{x}_\ominus$, are given by $\bar{p}_{\circledast} = \bar{x}_{\circledast} P_{\circledast}$. The momenta of the particles produced in the leading-order $N$-body process are $\bar{p}_i$, where $i$ ranges from 1 to $N$.

We use $\Phi_B$ to denote a set of variables defining a point in the $N$-body phase space and convolution over the incoming momentum fractions, and $\hat{\Phi}_B$ to denote a set of variables parametrizing the $N$-body phase space in the centre-of-mass frame of the partonic process. It will also be convenient to define $\bar{p}$ as the total momentum of the colour neutral particles, $\bar{p} \equiv \bar{x}_\oplus P_\oplus + \bar{x}_\ominus P_\ominus$, and $\bar{y}$ as the rapidity of $\bar{p}$. The partons' momentum fractions are therefore

$$\bar{x}_\oplus = \sqrt{\frac{\bar{p}^2}{s}} \mathrm{e}^{+\bar{y}}\,, \qquad\qquad \bar{x}_\ominus = \sqrt{\frac{\bar{p}^2}{s}} \mathrm{e}^{-\bar{y}}. \tag{3.1}$$

The phase space for the leading-order process is

$$\mathrm{d}\Phi_B \;=\; \mathrm{d}\bar{x}_\oplus\, \mathrm{d}\bar{x}_\ominus\, \mathrm{d}\hat{\Phi}_B \;=\; \frac{1}{s}\, \mathrm{d}\bar{p}^2\, \mathrm{d}\bar{y}\, \mathrm{d}\hat{\Phi}_B, \tag{3.2}$$

where $\mathrm{d}\hat{\Phi}_B$ is the Lorentz invariant phase space for the partonic process, in $n = 4 - 2\epsilon$ dimensions,

$$\mathrm{d}\hat{\Phi}_B = (2\pi)^n \prod_i \left[\mathrm{d}\bar{p}_i\right] \delta^n \left(\bar{p}_\oplus + \bar{p}_\ominus - \bar{p}\right)\,, \qquad\qquad \left[\mathrm{d}\bar{p}_i\right] = \frac{\mathrm{d}^{n-1}\bar{p}_i}{(2\pi)^{n-1}\, 2\bar{E}_i}\,, \tag{3.3}$$

and $s$ the hadronic centre-of-mass energy. The set of variables $\Phi_B = \left\{\bar{p}^2,\, \bar{y},\, \hat{\Phi}_B\right\}$ defines the *Born variables*.

The real emission corrections to the leading-order process consist of $2 \to N+1$ processes, $p_\oplus + p_\ominus \to p_1 + ... + p_N + k$, where we denote the momenta of the $N$ final-state colourless particles $p_i$ and that of the extra colour charged parton by $k$. The momentum fractions of the incoming partons are distinguished from those in the $2 \to N$ process as $x_\oplus$ and $x_\ominus$ ($p_{\circledast} = x_{\circledast} P_{\circledast}$). For these processes we introduce the Mandelstam variables $\hat{s}$, $\hat{t}$, $\hat{u}$ and the related *radiative variables* $\Phi_R = \{x,\, v,\, \phi\}$, which parametrize the extra emission:

$$\hat{s} = (p_\oplus + p_\ominus)^2 = \frac{p^2}{x}\,, \tag{3.4a}$$

$$\hat{t} = (p_\oplus - k)^2 \;= \frac{p^2}{x}\,(x-1)\,(1-v)\,, \tag{3.4b}$$

$$\hat{u} = (p_\ominus - k)^2 \;= \frac{p^2}{x}\,(x-1)\,v\,, \tag{3.4c}$$

where $\phi$ is the azimuthal angle of $k$ with respect to the $+z$ axis, and $p$ the total momentum of the colourless particles, $p \equiv x_\oplus P_\oplus + x_\ominus P_\ominus - k$.

To perform a simultaneous Monte Carlo sampling of the $N$- and $N$+1-body phase spaces one has to specify the integration variables. We choose two of these to be the mass and rapidity of the system of colourless particles, therefore $\bar{p}^2 \equiv p^2$ and $\bar{y} \equiv y$, where $y$ is defined by analogy to $\bar{y}$ as the rapidity of $p$.[7] The momentum fractions of the partons for $2 \to N+1$ processes are therefore related to those of the $2 \to N$ process by

$$x_\oplus = \frac{\bar{x}_\oplus}{\sqrt{x}} \sqrt{\frac{1-(1-x)(1-v)}{1-(1-x)v}}, \qquad x_\ominus = \frac{\bar{x}_\ominus}{\sqrt{x}} \sqrt{\frac{1-(1-x)v}{1-(1-x)(1-v)}}. \tag{3.5}$$

The phase space of the $N$+1-body real emission processes can be written in $n = 4-2\epsilon$ dimensions as

$$\mathrm{d}\Phi_{N+1} = \mathrm{d}\Phi_B \, \mathrm{d}\Phi_R \, \frac{p^2}{(4\pi)^2 x^2} \left(\frac{4\pi}{p^2}\right)^\epsilon \frac{1}{\Gamma(1-\epsilon)} \; \mathcal{J}(x,v), \tag{3.6}$$

where here the partonic Born variables $\hat{\Phi}_B$ specify a configuration in the rest frame of $p$ rather than $\bar{p}$. The function $\mathcal{J}(x,v)$ is given by

$$\mathcal{J}(x,v) = \left[\mathcal{S}\delta(1-x) + \mathcal{C}(x)\left(\delta(v) + \delta(1-v)\right) + \mathcal{H}(x,v)\right] \; v(1-v)(1-x)^2, \tag{3.7}$$

where

$$\mathcal{S} = \frac{1}{\epsilon^2} - \frac{\pi^2}{6}, \tag{3.8a}$$

$$\mathcal{C}(x) = -\frac{1}{\epsilon}\frac{1}{(1-x)_+} - \frac{1}{(1-x)_+}\ln x + 2\left(\frac{\ln(1-x)}{1-x}\right)_+, \tag{3.8b}$$

$$\mathcal{H}(x,v) = \frac{1}{(1-x)_+}\left(\frac{1}{v_+} + \frac{1}{(1-v)_+}\right). \tag{3.8c}$$

The labelling $\mathcal{S}, \mathcal{C}, \mathcal{H}$ reflects the fact that the $\mathcal{S}$ and $\mathcal{C}$ terms are multiplied by $\delta$-functions which limit their contributions to configurations with *soft* ($x \to 1$) and *collinear* ($v \to 0, 1$) emissions, while $\mathcal{H}$ is not associated with soft or collinear configurations but instead contributes to *hard* emissions[8] of the extra parton $k$.

The radiative phase space can be parametrized in terms of the radiative variables

$$\mathrm{d}\Phi_R = \frac{1}{2\pi}\,\mathrm{d}x\,\mathrm{d}v\,\mathrm{d}\phi, \tag{3.9}$$

where, in the partonic centre-of-mass frame, $x = 1 - k^0/E$, with $E$ the energy of either of the colliding partons, and $v = \frac{1}{2}(1+\cos\theta)$, with $\theta$ and $\phi$ the polar and azimuthal angles of $k$ with respect to the $+z$ axis.

As the rapidity of $p$ and $\bar{p}$ are equal, it is always possible to define a boost $\mathbb{B} = \mathbb{B}_L^{-1}\mathbb{B}_T\,\mathbb{B}_L$, such that $\mathbb{B}\; p = \bar{p}$, where $\mathbb{B}_L$ is a longitudinal boost to the frame in which $y = 0$ and $\mathbb{B}_T$ is a boost in the transverse direction, to the frame in which the transverse momentum of $p$ is zero. It follows that an $N$+1-body configuration can be assembled by first reconstructing

[7] Henceforth we will always refer to these variables as $p^2$ and $y$.

[8] Here by hard we simply mean emissions which are neither soft or collinear.

the $N$-body configuration corresponding to $\Phi_B$, then $p$ and $k$ (from $p^2$, $y$, $\Phi_R$), at which point the boost $\mathbb{B}$ can be calculated and its inverse applied to the $N$-body configuration. Although $\mathbb{B}_L$ is uniquely defined due to $p$ and $\bar{p}$ having the same rapidity, $y$, the transverse boost $\mathbb{B}_T$ can be modified according to $\mathbb{B}_T \to \mathbb{R}\mathbb{B}_T$, with $\mathbb{R}$ a rotation, and $\mathbb{B}$ will still satisfy $\mathbb{B}\, p = \bar{p}$. A convention must be adopted to fix $\mathbb{B}_T$, we shall return to this point later.

### 3.2 Matrix elements

The squared, spin and colour averaged leading-order matrix element for the $q + \bar{q} \to l + \bar{l}$ Drell-Yan process is given by $\mathcal{M}^B_{q\bar{q}}(p_q, p_{\bar{q}})$, where the first (second) argument refers to the incoming fermion (antifermion) momentum. The real emission radiative corrections consist of three processes: $q + \bar{q} \to l + \bar{l} + g$; $g + q \to l + \bar{l} + q$; and $g + \bar{q} \to l + \bar{l} + \bar{q}$. The matrix elements squared for these processes are given by

$$\mathcal{M}^R_{q\bar{q}} = \frac{\mathcal{N}_{q\bar{q}}}{p^2 \hat{t}\hat{u}} \Big[ \left(\hat{s}+\hat{t}\right)^2 \mathcal{M}^B_{q\bar{q}}(\tilde{p}_q, \tilde{p}_{\bar{q}g}) + \left(\hat{s}+\hat{u}\right)^2 \mathcal{M}^B_{q\bar{q}}(\tilde{p}_{qg}, \tilde{p}_{\bar{q}}) - \frac{1}{2}\epsilon \left(\hat{t}+\hat{u}\right)^2 \left(\mathcal{M}^B_{q\bar{q}}(\tilde{p}_g, \tilde{p}_{gg}) + \mathcal{M}^B_{q\bar{q}}(\tilde{p}_{gg}, \tilde{p}_g)\right) \Big], \tag{3.10a}$$

$$\mathcal{M}^R_{qg} = -\frac{\mathcal{N}_{qg}}{p^2 \hat{u}\hat{s}} \Big[ \left(\hat{t}+\hat{u}\right)^2 \mathcal{M}^B_{q\bar{q}}(\tilde{p}_{qg}, \tilde{p}_{\bar{q}}) + \left(\hat{t}+\hat{s}\right)^2 \mathcal{M}^B_{q\bar{q}}(\tilde{p}_q, \tilde{p}_{\bar{q}g}) - \frac{1}{2}\epsilon \left(\hat{u}+\hat{s}\right)^2 \left(\mathcal{M}^B_{q\bar{q}}(\tilde{p}_g, \tilde{p}_{gg}) + \mathcal{M}^B_{q\bar{q}}(\tilde{p}_{gg}, \tilde{p}_g)\right) \Big], \tag{3.10b}$$

$$\mathcal{M}^R_{g\bar{q}} = -\frac{\mathcal{N}_{qg}}{p^2 \hat{s}\hat{t}} \Big[ \left(\hat{u}+\hat{s}\right)^2 \mathcal{M}^B_{q\bar{q}}(\tilde{p}_{qg}, \tilde{p}_{\bar{q}}) + \left(\hat{u}+\hat{t}\right)^2 \mathcal{M}^B_{q\bar{q}}(\tilde{p}_q, \tilde{p}_{\bar{q}g}) - \frac{1}{2}\epsilon \left(\hat{s}+\hat{t}\right)^2 \left(\mathcal{M}^B_{q\bar{q}}(\tilde{p}_g, \tilde{p}_{gg}) + \mathcal{M}^B_{q\bar{q}}(\tilde{p}_{gg}, \tilde{p}_g)\right) \Big], \tag{3.10c}$$

where, for a more uniform notation, and to help show how the crossing of the leading-order process is manifest, we have denoted the final-state quark momentum in the $qg$ initiated process by $p_{\bar{q}}$ and the final-state antiquark momentum in the $g\bar{q}$ process by $p_q$. The shifted momenta $\tilde{p}_i$, $\tilde{p}_{jg}$, and the normalization constants $\mathcal{N}_{q\bar{q}}$, $\mathcal{N}_{qg}$ are given by

$$\begin{aligned} \tilde{p}_i &= \frac{1}{x_i} p_i \,, & \mathcal{N}_{q\bar{q}} &= 8\pi\alpha_S C_F \mu^{2\epsilon} \,, \\ x_i &= \frac{2p.p_i}{p^2} \,, & \mathcal{N}_{qg} &= 8\pi\alpha_S T_F \mu^{2\epsilon} / \left(1-\epsilon\right) \,, \\ \tilde{p}_{jg} &= p - \tilde{p}_i \,, \end{aligned} \tag{3.11}$$

where $\mu$ is the regularization scale emerging from the use of conventional dimensional regularization. The shifted momenta satisfy

$$\tilde{p}_i^2 = \tilde{p}_{jg}^2 = 0, \qquad \tilde{p}_i + \tilde{p}_{jg} = p, \tag{3.12}$$

*i.e.* they obey the relations required for them to be considered as describing a kinematic configuration for the leading-order process, hence they form valid arguments for $\mathcal{M}^B_{q\bar{q}}$.

These matrix elements hold independently of the type of exchanged vector boson, they also hold for the case that the leading-order process consists of interferences between

diagrams with different exchanged vector bosons. This universal behaviour is due to the factorisation of the NLO hadron tensor, into kinematic factors multiplying the leading-order hadron tensor. Such a factorisation of the matrix element is not necessary for the implementation of the POWHEG method but it improves the flexibility and generality of our implementation of the Drell-Yan process. This allows us generate $N$+1-body configurations, according to the full real emission matrix element, given the leading-order configuration using a technique of sampling the radiative phase space with a branching algorithm known as *the Kleiss trick* [13,42], which we have extended to $n$ dimensions as needed for a complete NLO calculation, as we now describe in detail.

The $\mathcal{O}(\alpha_S)$ virtual corrections to the $q+\bar{q} \to l+\bar{l}$ process solely consist of the $q\bar{q}$ vertex correction. At NLO, this loop diagram only contributes to the matrix element through its interference with the leading-order amplitude, correcting it by,

$$\mathcal{M}^V_{q\bar{q}} = \frac{\alpha_S C_F}{2\pi} \left(\frac{4\pi\mu^2}{p^2}\right)^{\epsilon} \frac{1}{\Gamma(1-\epsilon)} \left[-\frac{2}{\epsilon^2} - \frac{3}{\epsilon} - 8 + \pi^2\right] \mathcal{M}^B_{q\bar{q}}(p_q, p_{\bar{q}})\,. \tag{3.13}$$

### 3.3 Differential cross section

The partonic flux due to parton $a$ in hadron $A$ and parton $b$ in hadron $B$, at scale $\mu^2$, with momentum fractions $x_\oplus$ and $x_\ominus$ respectively, is defined as

$$\mathcal{L}_{ab}(x_\oplus, x_\ominus) = f_a^A\left(x_\oplus, \mu^2\right) f_b^B\left(x_\ominus, \mu^2\right). \tag{3.14}$$

In $\mathcal{L}_{ab}(x_\oplus, x_\ominus)$ the functions $f_i^I\left(x_i, \mu^2\right)$ are the parton distribution functions (PDFs) for finding a parton $i$ in hadron $I$ with momentum fraction $x_i$ at scale $\mu^2$. The contribution to the differential cross section from the leading-order process $q + \bar{q} \to l + \bar{l}$ is therefore

$$\mathrm{d}\sigma^B_{q\bar{q}} = B(\Phi_B)\,\mathrm{d}\Phi_B\,, \tag{3.15}$$

where

$$B(\Phi_B) = \frac{1}{2p^2}\,\mathcal{M}^B_{q\bar{q}}(\bar{p}_\oplus, \bar{p}_\ominus)\;\mathcal{L}_{q\bar{q}}(\bar{x}_\oplus, \bar{x}_\ominus)\,. \tag{3.16}$$

The virtual corrections (Eq. 3.13) add

$$\mathrm{d}\sigma^V_{q\bar{q}} = V_0(\Phi_B)\,\mathrm{d}\Phi_B\,, \tag{3.17}$$

where

$$V_0(\Phi_B) = \frac{\alpha_S C_F}{2\pi}\left[-\frac{2}{\epsilon}\left(\frac{1}{\bar{\epsilon}} + \ln\left(\frac{\mu^2}{p^2}\right)\right) - \frac{3}{\bar{\epsilon}} + \frac{\pi^2}{3} + \mathcal{V}_{q\bar{q}}\right] B(\Phi_B)\,, \tag{3.18}$$

with $\bar{\epsilon}$ defined by $\frac{1}{\bar{\epsilon}} = \frac{1}{\epsilon} - \gamma_E + \ln(4\pi)$ and

$$\mathcal{V}_{q\bar{q}} = -3\ln\left(\frac{\mu^2}{p^2}\right) + \frac{2\pi^2}{3} - 8\,. \tag{3.19}$$

In Eqs. 3.16 and 3.17 we have included a flux factor $1/2p^2$ for the partonic process. The subscript on $V_0$ identifies the bare divergent quantity.

The differential cross section for the real emission processes $a + b \to l + \bar{l} + c$ is of the form

$$\mathrm{d}\sigma^R_{ab} = \frac{1}{4\pi x}\ \mathcal{L}_{ab}\left(x_\oplus, x_\ominus\right)\ \left[\sum_i\ f_i\left(x,v\right)\ \mathcal{M}^B_{q\bar{q}}\left(\tilde{p}_i, \tilde{p}_j\right)\right]\ \mathrm{d}\Phi_B\ \mathrm{d}\tilde{\Phi}_R\,, \tag{3.20}$$

where for $i = qg,\ q,\ g,\ gg$, we have $j\left(i\right) = \bar{q},\ \bar{q}g,\ gg,\ g$. Each of the $f_i\left(x,v\right)$ functions is defined as the coefficient of the squared leading-order matrix element in the $\mathcal{M}^R_{ab}$ real-emission matrix element, Eq. 3.10.

Returning to the earlier discussion of the definition of the Born variables and the boost $\mathbb{B}$, we note that for each $i$ in Eq. 3.20 the boost to the rest frame of $\tilde{p}_i + \tilde{p}_j$ is the same up to an overall rotation (as $\tilde{p}_i + \tilde{p}_j = p$). Furthermore, for $i = q$ we have $\tilde{p}_i = p_i/x_i$, so $\tilde{p}_i$ and $p_i$ have the same orientation, as do $\tilde{p}_j$ and $p_j$ for index $j = \bar{q}$. Since $\mathbb{B}$ was defined up to an arbitrary rotation $\mathbb{R}$, we could choose to resolve this ambiguity by setting $\mathbb{R} = \mathbb{R}_q$, $\mathbb{B} = \mathbb{B}_q$, where $\mathbb{B}_q$ additionally satisfies,

$$\mathbb{B}_q\,\tilde{p}_q \equiv \mathbb{B}_L^{-1}\mathbb{R}_q\,\mathbb{B}_T\,\mathbb{B}_L\,\tilde{p}_q = \bar{p}_\oplus, \tag{3.21}$$

*i.e.* $\mathbb{R}_q$ is such that the value of $\tilde{p}_q$ in the $p$ rest frame is equal to $\bar{p}_\oplus$ in the $\bar{p}$ rest frame, therefore

$$\mathcal{M}^B_{q\bar{q}}\left(\tilde{p}_q, \tilde{p}_{\bar{q}g}\right)\mathrm{d}\Phi_B \equiv \mathcal{M}^B_{q\bar{q}}\left(\bar{p}_\oplus, \bar{p}_\ominus\right)\mathrm{d}\Phi_B. \tag{3.22}$$

To have the analogous equivalence for the $i,\ j = qg,\ \bar{q}$ term, one needs to have $\mathbb{B} = \mathbb{B}_{qg}$, defined such that $\mathbb{B}_{qg}\,\tilde{p}_{\bar{q}} = \bar{p}_\ominus$ is satisfied along with original requirement ($\mathbb{B}\,p = \bar{p}$).

Similar boosts can be constructed for the $i = g,\ gg$ terms in the matrix element, mapping $\tilde{p}_g$ to $\bar{p}_\oplus$ and $\bar{p}_\ominus$ respectively. However, as these terms carry a factor $\epsilon$, they only contribute to exactly collinear configurations in which the parton $k$ is *unresolved*, hence those boosts are a purely formal consideration, and are not needed in practice.

The real emission phase space can therefore be sampled using a simple Monte Carlo *branching algorithm*; namely, given a set of Born and radiative variables, the event is reconstructed as described in Sect. 3.1, except that, where previously a single boost $\mathbb{B}^{-1}$ was used to embed the $N$-body configuration in the $N$+1-body event, now we use a boost $\mathbb{B}_i^{-1}$ selected according to the probability distribution $\mathcal{P}_i = f_i\left(x,v\right)/\sum_i f_i\left(x,v\right)$. Sampling the phase space in this way, the generation of the Born variables becomes completely independent of the radiative variables:

$$\mathrm{d}\sigma^R_{ab} = R_{ab,0}\left(\Phi_B, \Phi_R\right)\ \mathrm{d}\Phi_R\,\mathrm{d}\Phi_B \tag{3.23a}$$

$$R_{ab,0}\left(\Phi_B, \Phi_R\right) = \frac{\hat{s}}{2\pi}\,\hat{\mathcal{L}}_{ab}\left(x_\oplus, x_\ominus\right)\sum_i\ f_i\left(x,v\right)\ \frac{\mathrm{d}\tilde{\Phi}_R}{\mathrm{d}\Phi_R}\,B\left(\Phi_B\right), \tag{3.23b}$$

where $\hat{\mathcal{L}}_{ab}$ is the ratio of the general parton flux relative to that of the leading-order process,

$$\hat{\mathcal{L}}_{ab}\left(x_\oplus, x_\ominus\right) = \frac{\mathcal{L}_{ab}\left(x_\oplus, x_\oplus\right)}{\mathcal{L}_{q\bar{q}}\left(\bar{x}_\oplus, \bar{x}_\ominus\right)}. \tag{3.24}$$

The functions $R_{ab,0}\left(\Phi_B, \Phi_R\right)$, calculated according to Eq. 3.23, are given by

$$R_{ab,0}\left(\Phi_B, \Phi_R\right) = \frac{\alpha_S C_{ab}}{2\pi}\,\frac{1}{x}\,\hat{\mathcal{L}}_{ab}\left(x_\oplus, x_\ominus\right)\ \mathcal{R}_{ab,0}\,B\left(\Phi_B\right), \tag{3.25}$$

where $C_{ab} = C_F$ for $ab = q\bar{q}$ and $T_F$ otherwise.

For the $q\bar{q}$ contribution $\mathcal{R}_{q\bar{q},0}$ is given by

$$\mathcal{R}_{q\bar{q},0} = \mathcal{S}_{q\bar{q}}\delta\left(1-x\right) + \left(-\frac{1}{\bar{\epsilon}}P_{qq} + \mathcal{C}_{q\bar{q}}\right)\left(\delta\left(v\right) + \delta\left(1-v\right)\right) + \mathcal{H}_{q\bar{q}}, \tag{3.26}$$

where

$$\mathcal{S}_{q\bar{q}} = \left(\frac{2}{\epsilon}+3\right)\left(\frac{1}{\bar{\epsilon}} + \ln\left(\frac{\mu^2}{p^2}\right)\right) - \frac{\pi^2}{3} - 3\ln\left(\frac{\mu^2}{p^2}\right), \tag{3.27a}$$

$$P_{qq} = \left(\frac{1+x^2}{1-x}\right)_+, \tag{3.27b}$$

$$\mathcal{C}_{q\bar{q}} = \left(1+x^2\right)\left(\frac{1}{\left(1-x\right)_+}\ln\left(\frac{p^2}{\mu^2 x}\right) + 2\left(\frac{\ln\left(1-x\right)}{1-x}\right)_+\right) + 1 - x, \tag{3.27c}$$

$$\mathcal{H}_{q\bar{q}} = \frac{1}{\left(1-x\right)_+}\left(\frac{1}{v_+} + \frac{1}{\left(1-v\right)_+}\right)\left(\left(1-x\right)^2\left(1-2v\left(1-v\right)\right) + 2x\right). \tag{3.27d}$$

For the $qg$ contribution $\mathcal{R}_{qg,0}$ is given by

$$\mathcal{R}_{qg,0} = \left(-\frac{1}{\bar{\epsilon}}\,P_{gq} + \mathcal{C}_{qg}\right)\delta\left(v\right) + \mathcal{H}_{qg}\,, \tag{3.28}$$

where

$$P_{gq} = x^2 + \left(1-x\right)^2\,, \tag{3.29a}$$

$$\mathcal{C}_{qg} = \left(x^2 + \left(1-x\right)^2\right)\left(\ln\left(\frac{p^2}{\mu^2 x}\right) + 2\ln\left(1-x\right)\right) + 2x\left(1-x\right)\,, \tag{3.29b}$$

$$\mathcal{H}_{qg} = \frac{1}{v_+}\left(2x\left(1-x\right)v + \left(1-x\right)^2 v^2 + x^2 + \left(1-x\right)^2\right). \tag{3.29c}$$

The function $\mathcal{R}_{g\bar{q},0}$ is equal to $\mathcal{R}_{qg,0}$ under the replacement $v \leftrightarrow 1-v$.

The soft term in the real correction $R_{q\bar{q},0}$, proportional to $\delta\left(1-x\right)$, is now combined with the virtual correction $V_0$, to give a soft-virtual contribution $V$, which is finite for $\epsilon \to 0$. The remaining divergences are initial-state collinear divergences proportional to $\delta\left(v\right)$ and/or $\delta\left(1-v\right)$. Working in the $\overline{\text{MS}}$ scheme these are absorbed into the definition of the PDFs. This renormalization and cancellation of divergences amounts to the replacements, $V_0 \to V$ and $R_{ab,0} \to R_{ab}$, where

$$V\left(\Phi_B\right) = \frac{\alpha_S C_F}{2\pi}\,\mathcal{V}_{q\bar{q}}\,B\left(\Phi_B\right) \tag{3.30}$$

and

$$R_{ab}\left(\Phi_B,\Phi_R\right) = \frac{\alpha_S C_{ab}}{2\pi}\,\frac{1}{x}\,\mathcal{R}_{ab}\,\hat{\mathcal{L}}_{ab}\left(x_\oplus, x_\ominus\right)\,B\left(\Phi_B\right), \tag{3.31a}$$

$$\mathcal{R}_{q\bar{q}}\left(\Phi_B,\Phi_R\right) = \mathcal{C}_{q\bar{q}}\left(\delta\left(v\right)+\delta\left(1-v\right)\right) + \mathcal{H}_{q\bar{q}}, \tag{3.31b}$$

$$\mathcal{R}_{qg}\left(\Phi_B,\Phi_R\right) = \mathcal{C}_{qg}\delta\left(v\right) + \mathcal{H}_{qg}, \tag{3.31c}$$

$$\mathcal{R}_{g\bar{q}}\left(\Phi_B,\Phi_R\right) = \mathcal{C}_{g\bar{q}}\delta\left(1-v\right) + \mathcal{H}_{g\bar{q}}. \tag{3.31d}$$

Adding these contributions we obtain the NLO differential cross section:

$$\mathrm{d}\sigma = B\left(\Phi_B\right)\mathrm{d}\Phi_B + V\left(\Phi_B\right)\mathrm{d}\Phi_B + R\left(\Phi_B,\Phi_R\right)\mathrm{d}\Phi_B\mathrm{d}\Phi_R\,, \tag{3.32}$$

where $R$ denotes the sum of the $R_{ab}$ terms.

## 4. Implementation in Herwig++

In the first two parts of this section we describe how distributions of NLO accurate non-radiative and single emission events are generated. In Sect. 4.3 we describe the simulation of further, lower $p_T$, emissions, from the radiative events, using the truncated and vetoed shower algorithms.

### 4.1 Generation of the leading-order configuration

As noted in Sect. 2, sampling the $\overline{B}(\Phi_B)$ function (Eq. 2.2), which is the next-to-leading order differential cross section integrated over the radiative variables,

$$\overline{B}(\Phi_B) = B(\Phi_B)\left[1 + \frac{\alpha_S C_F}{2\pi}\mathcal{V}_{q\bar{q}} + \sum_{ab}\int \mathrm{d}\Phi_R \frac{\alpha_S C_{ab}}{2\pi}\frac{1}{x}\mathcal{R}_{ab}\hat{\mathcal{L}}_{ab}(x_\oplus, x_\ominus)\right] \tag{4.1}$$

provides Born variables $\Phi_B$ distributed according to the exact NLO differential cross section. The way in which the leading-order process is factorised inside the real emission terms $R_{ab}$ allows the $\overline{B}(\Phi_B)$ distribution to be generated as a straightforward reweighting[9] of the leading-order cross section.

For convenience the radiative phase space $\mathrm{d}\Phi_R$ is reparametrized by variables on the interval $[0,1]$ such that the radiative phase space volume is unity, a three-dimensional unit cube. This is achieved by a trivial change of variables $\phi \to \bar{\phi} = \phi/2\pi$ and $x \to \tilde{x}$, where $\tilde{x}$ is defined by

$$x(\tilde{x}, v) = \bar{x}(v) + (1 - \bar{x}(v))\,\tilde{x}, \tag{4.2}$$

where $\bar{x}(v)$ is the lower limit on the $x$ integration. Numerical implementation of the $\overline{B}(\Phi_B)$ distribution requires all plus distributions be replaced by regular functions, the results of which are given in Appendix. A.

The generation of the leading-order, $N$-body configuration proceeds as follows:

1. a leading-order configuration is generated using the standard Herwig++ leading-order matrix element generator, providing the Born variables $\Phi_B$ with an associated weight $B(\Phi_B)$;

2. radiative variables $\Phi_R$ are then generated by sampling $\overline{B}(\Phi_B)$, parametrized in terms of the 'unit-cube' variables $\tilde{x}$, $v$, $\bar{\phi}$, using the Auto-Compensating Divide-and-Conquer (ACDC) phase space generator [43], which implements a variant of the VEGAS algorithm [44];

3. the leading-order configuration is accepted with a probability proportional to the integrand of Eq. 4.1 evaluated at $\{p^2, y, \Phi_R\}$.

[9] Apart from the requirement that the final state be colour neutral, this reweighting is independent of the details of the vector boson and any decay it undergoes.

### 4.2 Generation of the hardest emission

The hardest (highest $p_T$) emission is generated from the $N$-body configuration according to the modified Sudakov form factor, Eq. 2.3. The integrand in the exponent of the Sudakov form factor consists of three different contributions, one for each channel $ab$=$q\bar{q}$, $qg$, $g\bar{q}$. The integrands are defined as

$$W_{ab}\left(\Phi_R, \Phi_B\right) = \frac{\hat{R}_{ab}\left(\Phi_B, \Phi_R\right)}{B\left(\Phi_B\right)} = \frac{\alpha_S C_{ab}}{2\pi}\,\frac{1}{x}\,\hat{\mathcal{H}}_{ab}\,\hat{\mathcal{L}}_{ab}\left(x_\oplus, x_\ominus\right), \tag{4.3}$$

where $\hat{\mathcal{H}}_{ab}$ is equal to $\mathcal{H}_{ab}$ without the plus prescription. We use the following parametrization of the partonic, vector boson and jet momentum in the hadronic centre-of-mass frame:

$$\begin{aligned} p_\oplus &= \frac{1}{2}\sqrt{s}\left(x_\oplus, 0, 0, +x_\oplus\right), \quad p = \left(m_T\cosh y, \quad p_T\sin\phi, \quad p_T\cos\phi, \, m_T\sinh y\right), \\ p_\ominus &= \frac{1}{2}\sqrt{s}\left(x_\ominus, 0, 0, -x_\ominus\right), \quad k = \left(p_T\cosh y_k, \, -p_T\sin\phi, \, -p_T\cos\phi, \, p_T\sinh y_k\right), \end{aligned} \tag{4.4}$$

where $p_T$ is the transverse momentum, $m_T = \sqrt{p^2 + p_T^2}$ and $y_k$ is the rapidity of the additional parton. Instead of generating the hardest emission in terms of $\Phi_R = \{x, v, \phi\}$ we find it more convenient to make a change of variables to $\Phi'_R = \{p_T, y_k, \phi\}$, related to $\Phi_R$ according to

$$p_T^2 = \frac{p^2}{x}\,v\left(1-v\right)\left(1-x\right)^2, \quad y_k = y + \frac{1}{2}\ln\left(\frac{v}{1-v}\right) - \frac{1}{2}\ln\left(\frac{1-v\left(1-x\right)}{x+v\left(1-x\right)}\right). \tag{4.5}$$

The modified Sudakov form factor of Eq. 2.3 contains a $\theta$-function in $p_T$, however by choosing to parametrize the radiative phase space in $p_T$ the $\theta$-function simply becomes the upper limit on the integral. The modified Sudakov form factor for each channel therefore has the form

$$\Delta_{\hat{R}_{ab}}\left(p_T\right) = \exp\left(-\int_{p_T}^{p_{T\max}} \mathrm{d}\Phi_R \; W_{ab}\left(\Phi_R, \Phi_B\right)\right), \tag{4.6}$$

where $p_{T\max}$ is the maximum possible transverse momentum. The full Sudakov form factor, $\Delta_{\hat{R}}(p_T)$, is given by the product of $\Delta_{\hat{R}_{ab}}(p_T)$ for the individual channels. The radiative variables ($p_T$, $y_k$) are generated according to Eq. 2.3 using the *veto algorithm*.[10] This procedure requires simple bounding functions for each channel. Functions of the form,

$$g_{ab}\left(p_T\right) = \frac{K_{ab}}{p_T^2}, \tag{4.7}$$

are used, with suitable values of $K_{ab}$ for each channel together with an overestimate of the limits for the rapidity integral, $y_{k_{\min}}$ and $y_{k_{\max}}$. The generation procedure then proceeds as follows:

1. $p_T$ is set to $p_{T\max}$;

[10] A good description of this technique can be found in Ref. [1].

2. a new ($p_T$, $y_k$) configuration is generated using two random numbers according to[11]

$$p_T = \left( \frac{1}{p_T} - \frac{1}{K_{ab}\left(y_{k_{\max}} - y_{k_{\min}}\right)} \ln \mathcal{R} \right)^{-1}, \tag{4.8a}$$

$$y_k = y_{k_{\min}} + \mathcal{R}\left(y_{k_{\max}} - y_{k_{\min}}\right); \tag{4.8b}$$

3. if $p_T < p_{T\min}$, where $p_{T\min}$ is the minimum allowed $p_T$ for the emission, then no radiation is generated;

4. if the generated configuration is outside of the exact phase space boundaries then return to step 2;

5. if $W_{ab}\left(\Phi_B, \Phi_R\right) / g_{ab}\left(p_T\right) > \mathcal{R}$ then accept the configuration, otherwise return to step 2.

For this process there are three partonic channels contributing to the radiative corrections, this is dealt with by using *competition*, where a ($p_T$, $y_k$) configuration is generated, as outlined above, for each channel individually and the configuration with the highest $p_T$ accepted.

We employ a simple prescription [13] to generate the azimuthal angle that allows the leptonic correlations to be correctly generated. For the $q\bar{q}$ channel, the prescription proceeds as follows:

1. momenta are first constructed in the vector boson rest frame;

2. the $p_\oplus$ direction is chosen with probability

$$\left(\hat{s}+\hat{t}\right)^2 / \left(\left(\hat{s}+\hat{t}\right)^2 + \left(\hat{s}+\hat{u}\right)^2\right), \tag{4.9}$$

   otherwise the $p_\ominus$ direction is chosen. The momenta are then rotated around the chosen direction by a random angle generated uniformly on the interval $[0, 2\pi]$;

3. momenta are boosted back to the lab frame such that the rapidity of the vector boson is the same as for the $N$-body configuration.

The same procedure is used for the $qg$ and $g\bar{q}$ initiated channels with the replacements $\hat{s} \to \hat{t}$, $\hat{t} \to \hat{u}$, $\hat{u} \to \hat{s}$ and $\hat{s} \to \hat{u}$, $\hat{t} \to \hat{s}$, $\hat{u} \to \hat{t}$, respectively.

### 4.3 Truncated and vetoed parton showers

Before describing how the radiative events are further showered, we need to recall some details of the Herwig++ parton shower algorithm. This is described in more detail in Refs. [18, 39]. The shower starts at a scale given by the colour structure of the hard scattering process and evolves down in the evolution variable $\tilde{q}$ by the emission of partons in $1 \to 2$ branching processes. Finally, the set of scales, $\tilde{q}$, momentum fractions, $z$, and azimuthal angles, $\phi$, which describe these branchings, are used to construct the momenta of

[11] $\mathcal{R}$ refers to a random number in the interval $[0, 1]$, a different random number is generated each time.

all the partons radiated in the parton shower. The Herwig++ approach generally requires some reshuffling of these momenta after the generation of the parton showers in order to ensure global energy-momentum conservation.

The $N$+1-body states generated as described in Sect. 4.2 are first interpreted as a single standard Herwig++ shower emission, from the $N$-body configuration, described by the shower branching variables ($\tilde{q}_h$, $z_h$, $\phi_h$). The complete POWHEG shower is then performed as a single Herwig++ shower modified by certain conditions which allows a simple but complete implementation of the truncated shower.

The shower algorithm proceeds as follows:

1. the truncated shower evolves from the hard scale, determined by the colour structure of the $N$-body process, to the hardest emission scale $\tilde{q}_h$ such that the $p_T$ is less than that of the hardest emission, the radiation is angular-ordered and branchings do not change the flavour of the emitting parton;

2. the hardest emission is forced with shower variables ($\tilde{q}_h$, $z_h$, $\phi_h$);

3. the shower is allowed to evolve down to the hadronization scale with the addition of a transverse momentum veto on radiation above $p_{T_h}$.

The implementation described above requires that the hardest emission, generated as described in Sect. 4.2, be interpreted as a Herwig++ shower emission that is forced when we evolve to the associated scale in the parton shower. In order to do this, we need to find a mapping from the $N+1$ momenta, describing the hardest emission, to the shower variables ($\tilde{q}_h$, $z_h$, $\phi_h$) and an $N$-body configuration. This equates to undoing the momentum reconstruction procedure used in the Herwig++ shower. The reconstruction procedure consists of two steps [39]. First, the momenta of partons at each step of the shower are constructed, in the centre-of-mass frame of the hadronic collision, recursively from the shower variables. Second, boosts are applied to each jet individually which ensures global momentum conservation. The reconstruction process is different for initial- and final-state radiation, here we will only consider the initial-state case which is relevant for the Drell Yan process.

In Herwig++ the momenta of the partons, $q_i$, in a jet are given by

$$q_i = \alpha_i p + \beta_i n + q_{\perp i}, \tag{4.10}$$

where for initial-state radiation the reference vectors $p$ and $n$ are given by the hadronic momenta of the beam particles $p_\oplus$ and $p_\ominus$ and $q_{\perp i}$ is the transverse momentum with respect to the beam axis.

For initial-state radiation we use a backward evolution algorithm which starts from the hard process and evolves to lower evolution scales backwards towards the incoming hadron by the emission of time-like partons. The reconstruction of the initial-state jet starts from the last initial-state parton produced by the backward evolution algorithm with momentum calculated from the fraction of the beam momentum it carries. The momentum of the time-like daughter of this parton is reconstructed as described in Ref. [39]. The momentum of the space-like daughter is then given by momentum conservation. This process is iterated

for each initial-state branching eventually giving the momentum of the space-like progenitor parton, colliding in the hard process.

The momenta of the two progenitor partons are then reshuffled such that mass and rapidity of the partonic centre-of-mass system is conserved. Under this reshuffling the progenitor momenta are transformed according to

$$q_{\circledast} \to q'_{\circledast} = \alpha_{\circledast} k_{\circledast} p_{\circledast} + \frac{\beta_{\circledast}}{k_{\circledast}} p_{\circledcirc} + q_{\perp\circledast}. \tag{4.11}$$

The reshuffling parameters, $k_\oplus$ and $k_\ominus$, are found by solving equations requiring conservation of mass and rapidity and hence the associated Lorentz transform is obtained.

The basis vectors are the hadronic beam momenta and the $\alpha_{\circledast}$ parameters in Eq. 4.11 are simply the Born partonic momentum fractions, given in Eq. 3.2. The reshuffling parameters, $k_{\circledast}$, can therefore be calculated from the momenta of the shuffled progenitors, $q'_{0\circledast}$. Decomposing these momenta into their Sudakov parameters the momentum shuffling parameters are simply

$$k_\oplus = \frac{\alpha'_{0\oplus}}{\bar{x}_\oplus}, \qquad\qquad k_\ominus = \frac{\alpha'_{0\ominus}}{\bar{x}_\ominus}, \tag{4.12}$$

where $\alpha'_{0\circledast}$ refers to the $\alpha$ parameters in the Sudakov decomposition of the shuffled progenitors. The inverse of the Lorentz boosts implementing the reshuffling can then be calculated and applied to each momentum, yielding the unshuffled momenta $q_i$. These are then decomposed yielding their Sudakov parameters, the shower variables parametrizing the branching can then be determined. The momentum fraction is given by

$$z = \frac{\alpha_i}{\alpha_{\tilde{ij}}}, \tag{4.13}$$

where $\alpha_i$ is the Sudakov parameter for the space-like parton entering the hard process and $\alpha_{\tilde{ij}}$ the Sudakov parameter of the initial-state parent parton. In this simple case the transverse momentum is simply equal to that of the off-shell space-like parton initiating the leading-order hard process, or equivalently, its outgoing, time-like, sister parton. The scale of the branching is defined in terms of the $p_T$ and light-cone momentum fraction $z$, as

$$\tilde{q}^2 = \frac{z Q_g^2 + p_T^2}{(1-z)^2}, \tag{4.14}$$

where $Q_g$ is the constituent gluon mass, the infrared regulator of the Herwig++ parton shower.

Using this approach we can calculate the shower variables $(\tilde{q}_h, z_h, \phi_z)$ for the hardest emission which allows us to generate the truncated and vetoed showers.

## 5. Results

As a check of the calculation of the next-to-leading order differential cross section, distributions of the vector boson rapidity produced by the POWHEG implementation and the

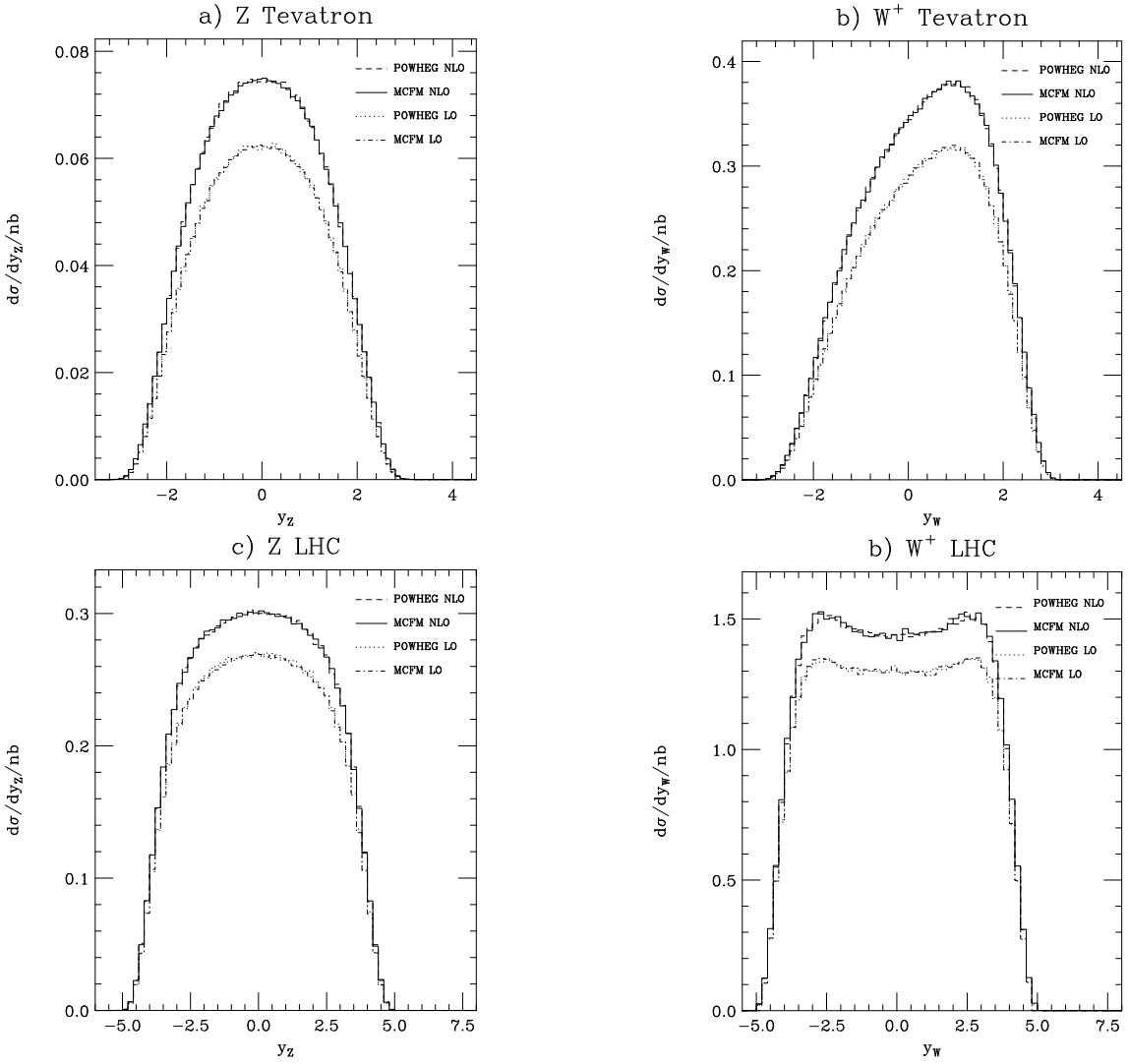


**Figure 1:** Comparisons of $\mathrm{d}\sigma/\mathrm{d}y$ for the POWHEG implementation and MCFM [45] for $Z$ and $W^+$ production at the Tevatron ($\sqrt{s} = 2$TeV) and the LHC ($\sqrt{s} = 14$TeV).

NLO program MCFM [45] were compared. Fig. 1 shows distributions for $\gamma/Z$ and $W^+$ production at the Tevatron (proton-antiproton at $\sqrt{s} = 2\,\mathrm{TeV}$) and the LHC (proton-proton at $\sqrt{s} = 14\,\mathrm{TeV}$). In all cases the total cross sections from MCFM and our POWHEG implementation agreed to within 0.5 %. The distribution of the rapidity of the lepton produced in the $\gamma/Z$ and $W$ decay is shown in Fig. 2 and is also in good agreement. For both Herwig++ and MCFM in this comparison, the parton density functions used were the MRST2001 NLO [46] set with the LHAPDF interface [47].

In Figs. 3-6, distributions from the Drell-Yan POWHEG implementations for the rapidity and transverse momentum of the vector bosons are compared to Tevatron data. The middle and bottom panels in each of these plots shows the (Theory − Data)/Data and $\chi$ values for each bin. In Fig. 3 the rapidity distribution of $\gamma/Z$ bosons of mass 71-111 GeV is compared to D0 Run II data [48]. Fig. 4 shows the transverse momentum distribu-

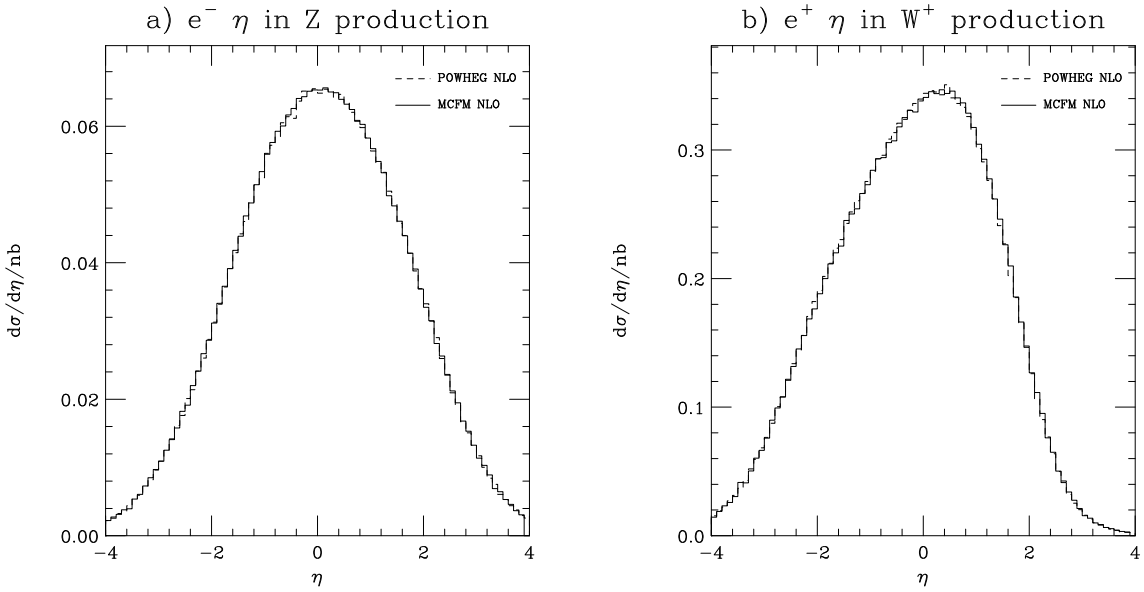


**Figure 2:** The rapidity of a) the electron in $Z$ and b) the positron in $W^+$ production at the Tevatron including the leptonic decay of the gauge boson for the POWHEG implementation and MCFM [45] at the Tevatron ($\sqrt{s} = 2$TeV).

tion of $\gamma/Z$ bosons of mass 66-116 GeV compared to CDF Run I data [49]. Fig. 5 shows the transverse momentum distribution of $\gamma/Z$ bosons of mass 40-200 GeV compared to D0 Run II data [50]. Fig. 6 shows the transverse momentum distribution of $W$ bosons compared to Run I D0 data [51]. In addition to the results from our implementation of the POWHEG method the results from Herwig++ including a matrix element correction and MC@NLO [19–24] are shown. The predicted $W$ and $Z$ $p_T$ distributions at the LHC are shown in Fig. 7.

The Herwig++ results were generated using an intrinsic $p_T$ of 2.2 GeV which was obtained by fitting to the Run I $W$ and $Z$ $p_T$ distributions [39]. The POWHEG results used the same intrinsic $p_T$ as for Herwig++ and a minimum $p_T$ of 2 GeV for the hardest emission. The MC@NLO and HERWIG results were generated using an intrinsic $p_T$ of 1.6 GeV from a fit to D0 data [52].

The leading-order parton distribution functions of [46] were used for the Herwig++ result and the central value of the NLO parton distributions of [53] for the POWHEG and MC@NLO results.

All the approaches give good agreement for the rapidity of the $Z$ boson however they differ in the description of the $p_T$ spectrum of the gauge boson. The chi squared per degree of freedom for the various $p_T$ spectra and approaches are given in Table 1. All the approaches are in good agreement with the Run I data from CDF and D0 for the $p_T$ of the $Z$ and $W$. However, with the exception of the results of the FORTRAN HERWIG program including a matrix element correction, which gave the worst agreement with the Run I $Z$ data, all the results are below the new D0 $Z$ $p_T$ data at high transverse momentum.

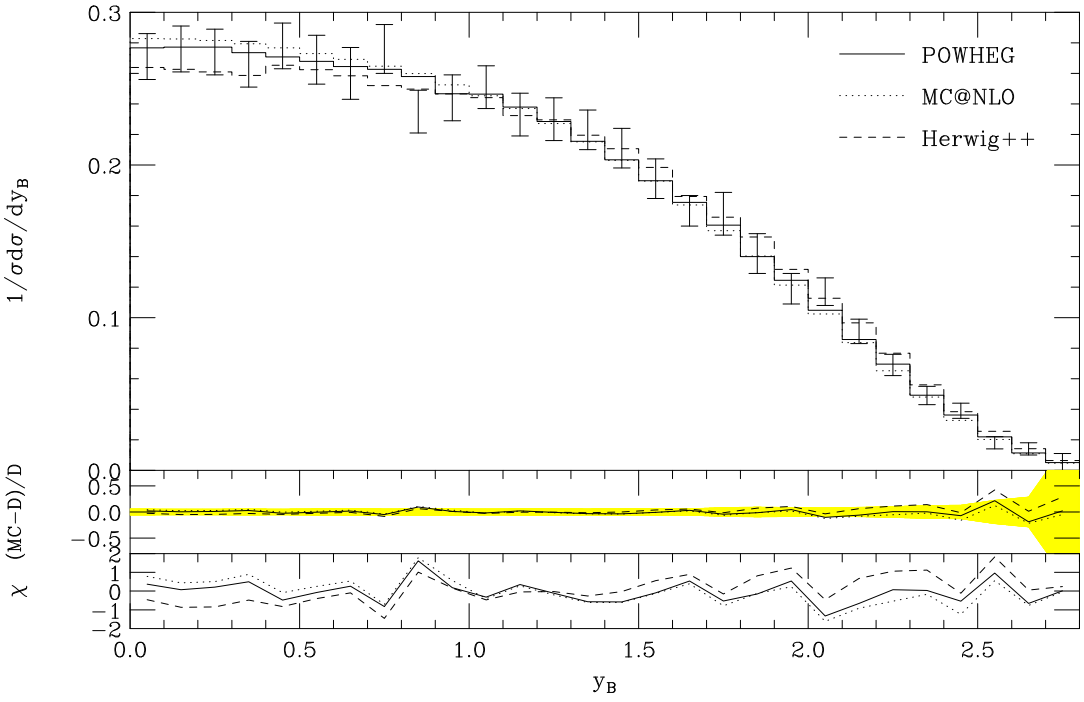


**Figure 3:** Rapidity distribution for $Z$ production compared to D0 Run II Tevatron data [48]. The solid line shows the prediction of our POWHEG implementation, the dotted line is the prediction of MC@NLO and the dashed line is the default Herwig++ result.

There is a common trend, at both the Tevatron and LHC energies, that the matrix element correction gives the largest result at large $p_T$, followed by the POWHEG approach with MC@NLO giving the lowest value. This is due to the treatment of the hardest emission in the different approaches. In the MC@NLO method the result at large $p_T$ is the leading-order matrix element for the production of a vector boson and a hard QCD jet. However in this region, as we are normalising to the total cross section, the matrix element correction result is essentially the matrix element for vector boson plus jet production multiplied by the K-factor[12] giving a larger result. In the large $p_T$ region the POWHEG result, because the real-emission matrix element is exponentiated, is the real-emission matrix element multiplied by the $\bar{B}$ function, which results in a K-factor-like correction, and the Sudakov form factor which causes the result to be slightly smaller than the default Herwig++ result. The POWHEG result has the significant advantage that rather than using a global rescaling of the cross section to get the NLO normalization, which can lead to a poor description of observables, such as the boson rapidity, which are non-zero at leading order the NLO correction is calculated for each momentum configuration.

In an ideal world we would like to use the NLO result for vector boson production in association with a hard jet to describe the high $p_T$ region, however incorporating this result into a Monte Carlo simulation is not currently feasible, and therefore the POWHEG

[12] The K-factor here is the ratio of the NLO cross section for inclusive vector boson production divided by the leading-order cross section.

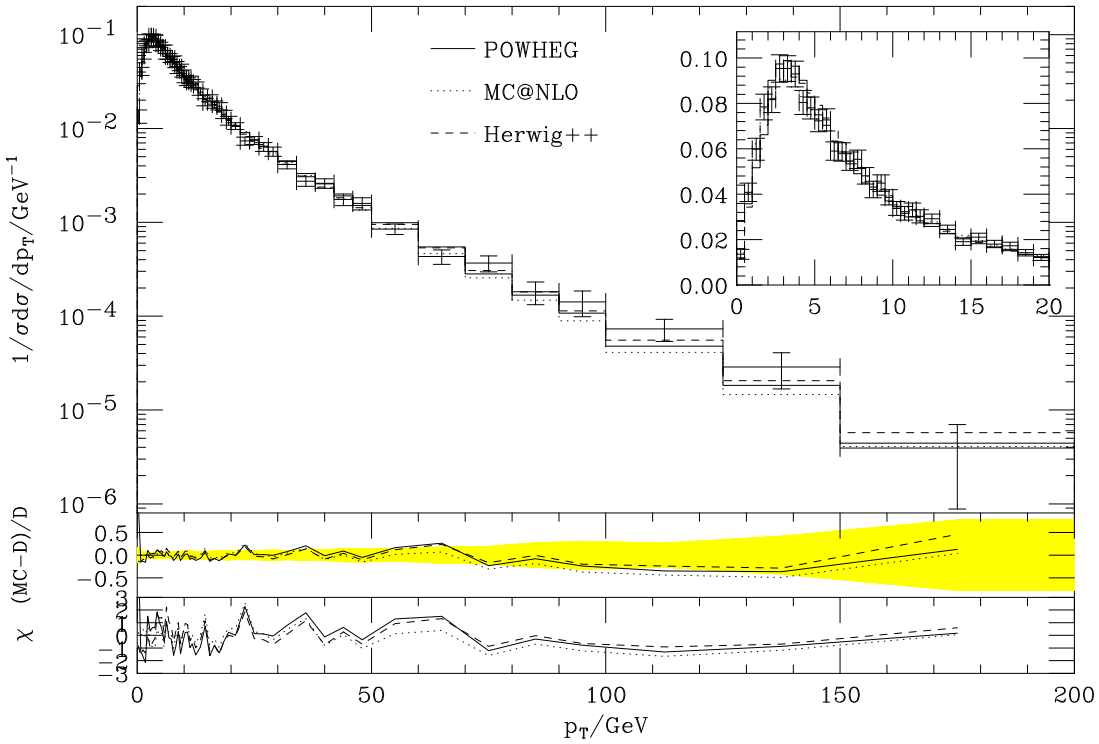


**Figure 4:** Transverse momentum distribution for $Z$ production compared to CDF Run I Tevatron data [49]. The solid line shows the prediction of our POWHEG implementation, the dotted line is the prediction of MC@NLO and the dashed line is the default Herwig++ result. The inset shows an expanded view of the low $p_T$ region.

| Approach | Data Set | | | | | |
|---|---|---|---|---|---|---|
| | D0 W $p_T$ | | CDF Z $p_T$ | | D0 Z $p_T$ | |
| | All | $p_T > 30\,\text{GeV}$ | All | $p_T > 30\,\text{GeV}$ | All | $p_T > 30\,\text{GeV}$ |
| MC@NLO | 0.51 | 0.82 | 0.70 | 0.96 | 7.2 | 13.9 |
| Herwig++ | 0.67 | 0.42 | 0.89 | 0.61 | 5.1 | 7.0 |
| POWHEG | 0.54 | 0.33 | 1.99 | 1.00 | 5.3 | 6.9 |
| HERWIG | 0.69 | 1.08 | 2.45 | 4.47 | 2.0 | 1.9 |

**Table 1:** Chi squared per degree of freedom for MC@NLO, Herwig++, our implementation of the POWHEG method in Herwig++ and FORTRAN HERWIG compared to Tevatron vector boson $p_T$ data. The chi-squared values are calculated for the shapes of the distributions, *i.e.* normalizing them to unity. In order to compare the high $p_T$ region and minimise the effect of tuning the intrinsic transverse momentum the chi squared per degree of freedom is given for both the full $p_T$ region and only for the data points with $p_T > 30\,\text{GeV}$.

or matrix element correction methods which basically assume the correction for inclusive production is the same as for vector boson production in association with a jet at least have the advantage of including a correction which improves agreement with data.

In general all the results lie below the D0 Run II $Z$ $p_T$ data between 50 and 100 GeV which results in the relatively poor chi squared, however in general the POWHEG approach

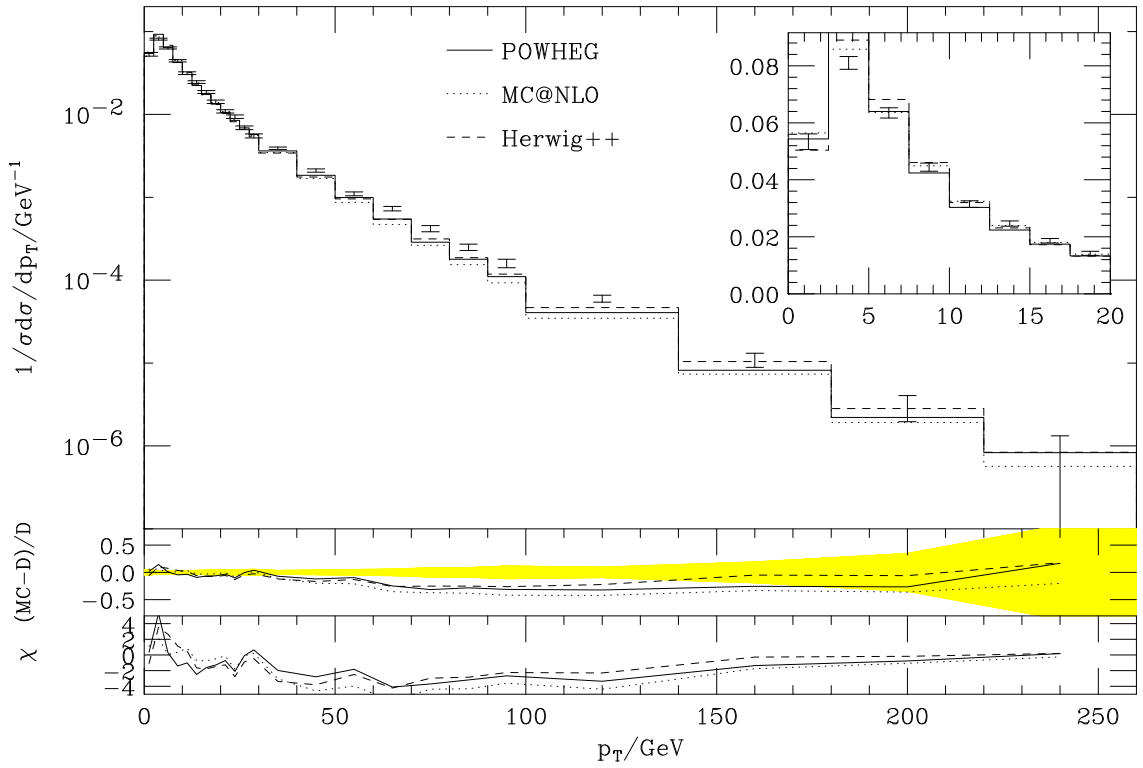


**Figure 5:** Transverse momentum distribution for $Z$ production compared to D0 Run II Tevatron data [50]. The solid line shows the prediction of our POWHEG implementation, the dotted line is the prediction of MC@NLO and the dashed line is the default Herwig++ result. The inset shows an expanded view of the low $p_T$ region.

gives comparable results to the other state-of-the-art techniques. The effect of varying the scale used for the parton distributions and $\alpha_S$ between $0.5\hat{s}$ and $2\hat{s}$ for the $\overline{B}$ term and between $0.5(M_B^2 + p_T^2)$ and $2(M_B^2 + p_T^2)$ for the hardest emission is shown in Fig. 8. While this variation moves the POWHEG result close to the data it still is below the experimental result in the intermediate $p_T$ region.

The effect of the truncated shower is illustrated in Fig. 9 which shows the small $p_T$ region of the transverse momentum distribution for $W$ and $Z$ production compared to D0 and CDF data. In this region where the highest $p_T$ emission is at a small scale and there is often a large region for the evolution of the truncated shower it has the largest effect. However the effect is relatively small at least for the transverse momentum distribution, equivalent to a small change in the intrinsic transverse momentum. We would expect to see a larger effect in the distributions of jets in the event, in particular the second hardest jet, which we will study in the future.

## 6. Conclusion

The POWHEG NLO matching prescription has been implemented in the Herwig++ Monte Carlo event generator for Drell-Yan vector boson production. A full treatment of the

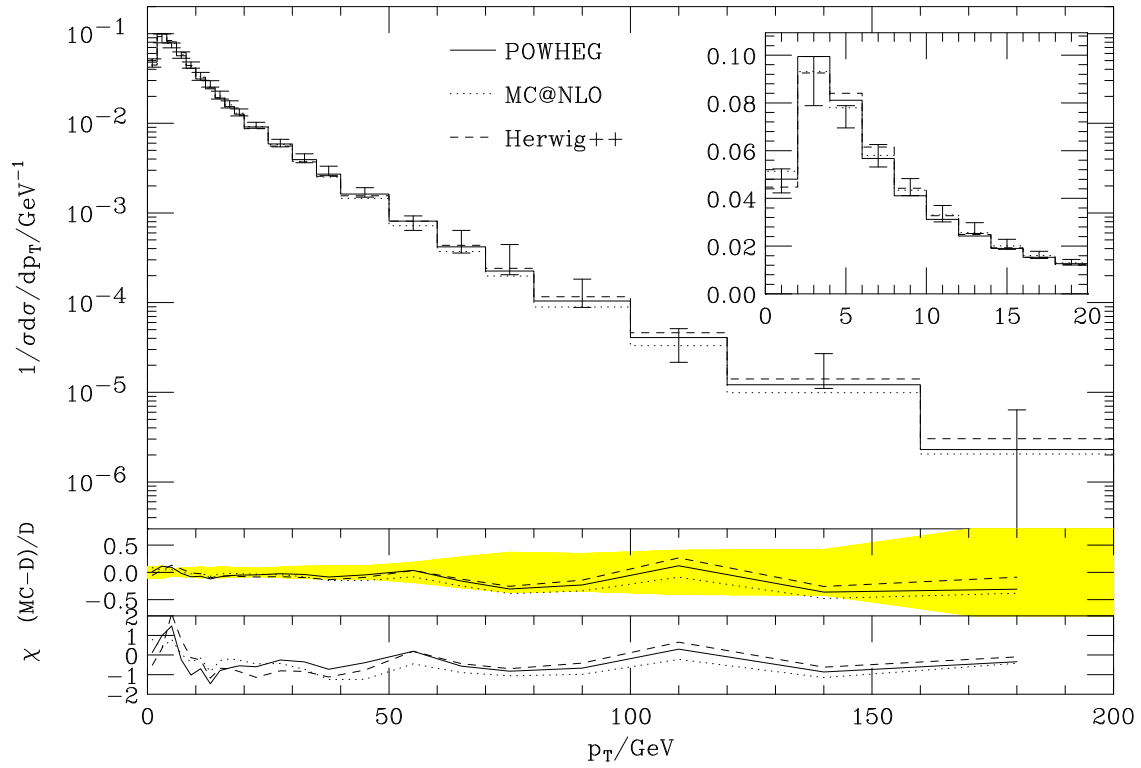


**Figure 6:** Transverse Momentum distribution for $W$ production compared to D0 Run I data [51]. The solid line shows the prediction of our POWHEG implementation, the dotted line is the prediction of MC@NLO and the dashed line is the default Herwig++ result. The inset shows an expanded view of the low $p_T$ region.

truncated shower, which is required to produce wide angle, soft radiation in angular-ordered parton showers, is included for the first time.

The implementation gives a good description of data, on a similar level to the matrix element correction methods and better than MC@NLO. It will be available in a forthcoming release of Herwig++.

The technique we have used to implement the POWHEG approach, by interpreting the hard emission in terms of the variables used to generate the parton shower is very powerful, and has many other applications in matching approaches, for example for the CKKW approach [32,33], which we will explore in the future.

## Acknowledgments

We are grateful to the other members of the Herwig++ collaboration and Paolo Nason for many useful discussions. We are particularly grateful to Mike Seymour for his careful reading of this manuscript. This work was supported by the Science and Technology Facilities Council, formerly the Particle Physics and Astronomy Research Council, the European Union Marie Curie Research Training Network MCnet under contract MRTN-CT-2006-

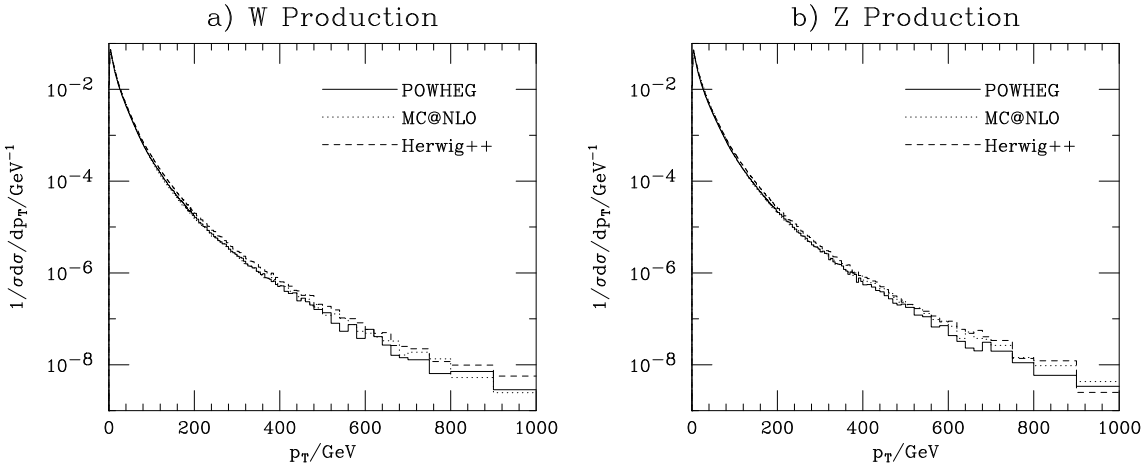


**Figure 7:** The $p_T$ distributions of a) $W$ and b) $Z$ bosons at the LHC. The solid line shows the prediction of our POWHEG implementation, the dotted line is the prediction of MC@NLO and the dashed line is the default Herwig++ result.

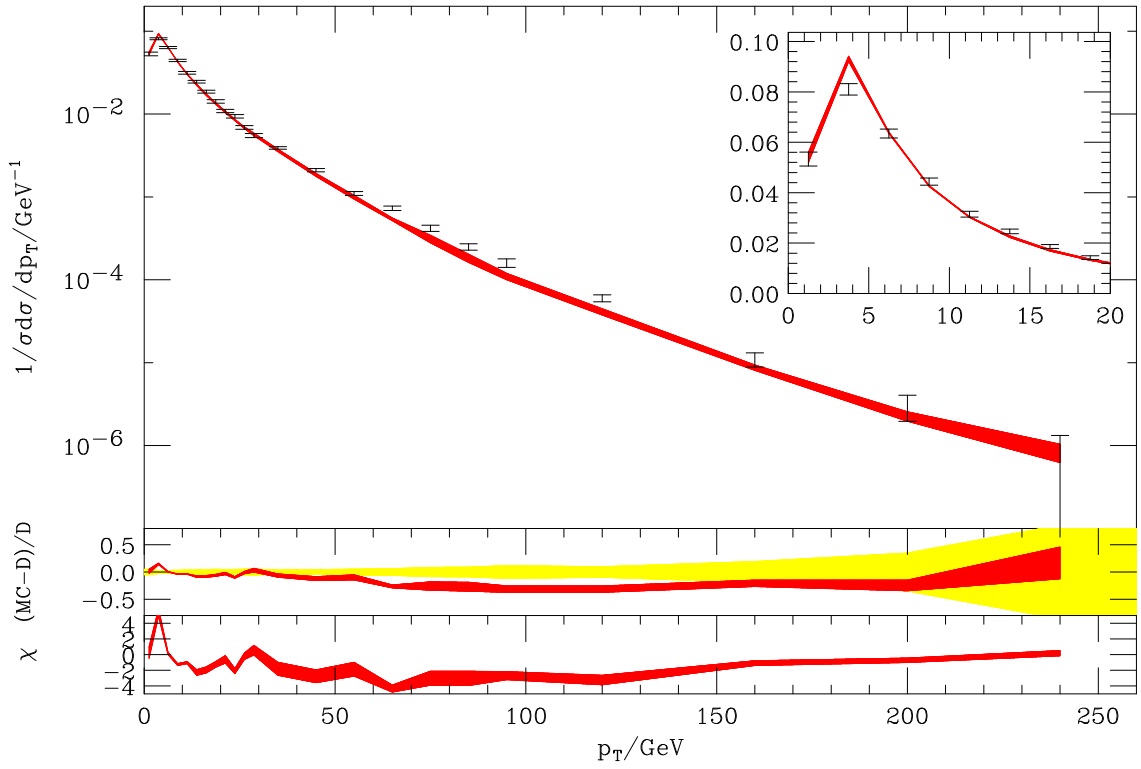


**Figure 8:** Transverse Momentum distribution for $Z$ production compared to D0 Run II data [50]. The band shows the effect of varying the scale used for the parton distributions and $\alpha_S$ between $0.5\hat{s}$ and $2\hat{s}$ for the $\overline{B}$ term and between $0.5(M_B^2 + p_T^2)$ and $2(M_B^2 + p_T^2)$ for the hardest emission.

035606. K. Hamilton acknowledges support from the Belgian Interuniversity Attraction Pole, PAI, P6/11.

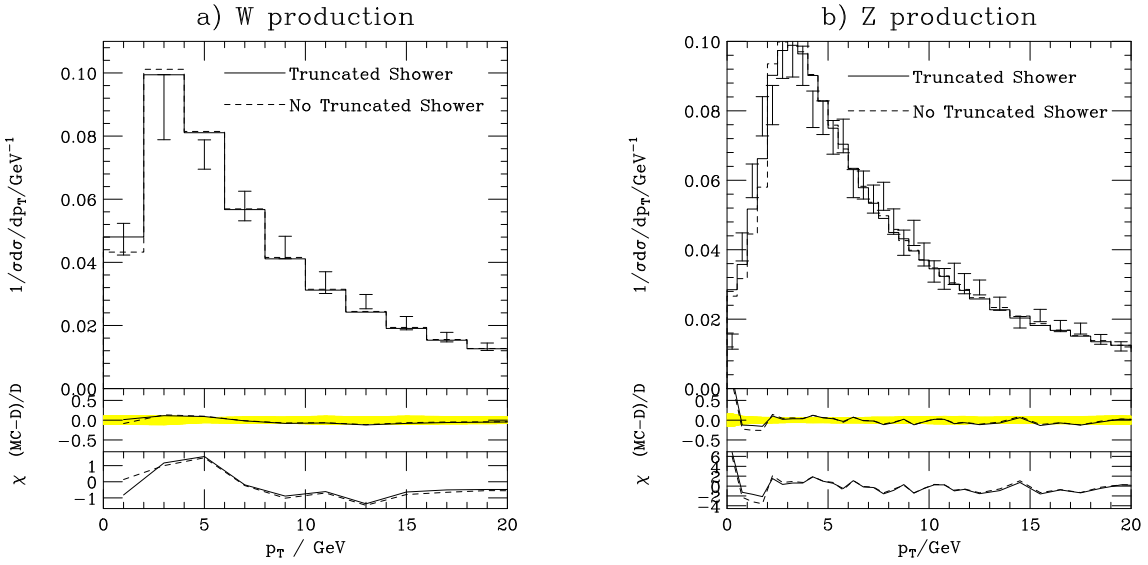


**Figure 9:** Transverse Momentum distribution for a) $W$ production compared to D0 Run I data [51] and b) $Z$ production compared to CDF Run I Tevatron data [49]. The solid line includes the truncated shower whereas the dashed line does not.

## Note added in Proof

While we were in the final stages of completing this paper another paper on the same topic was submitted to the arXiv [54].

## A. Plus Distributions

In order to implement the collinear ($\mathcal{C}_{ab}$) terms in the real-emission contributions to $\overline{B}\left(\Phi_B\right)$ the following relations are required

$$\int_{\bar{x}(v)}^{1} \mathrm{d}x \, \frac{f(x)}{(1-x)_+} = \int_0^1 \mathrm{d}\tilde{x} \; \left(1-\bar{x}\left(v\right)\right) \left[\frac{f(x(\tilde{x},v))-f(x(1,v))}{1-x(\tilde{x},v)} + \frac{f(x(1,v))}{1-\bar{x}(v)} \ln\left(1-\bar{x}\left(v\right)\right)\right] \tag{A.1}$$

and

$$\begin{aligned} &\int_{\bar{x}(v)}^{1} \mathrm{d}x \; f\left(x\right) \left(\frac{\ln(1-x)}{1-x}\right)_+ \\ &= \int_0^1 \mathrm{d}\tilde{x} \; \left(1-\bar{x}\left(v\right)\right) \left[\left(f\left(x\left(\tilde{x},v\right)\right) - f\left(x\left(1,v\right)\right)\right) \left(\frac{\ln(1-x(\tilde{x},v))}{1-x(\tilde{x},v)}\right) + \frac{f(x(1,v))}{2(1-\bar{x}(v))} \ln^2\left(1-\bar{x}\left(v\right)\right)\right] \end{aligned} \tag{A.2}$$

with $\tilde{x}$ defined in Eq. 4.10 and $v \in [0,1]$. For the hard ($\mathcal{H}_{ab}$) contribution to the real radiation components in $\overline{B}\left(\Phi_B\right)$

$$\begin{aligned} &\int_0^1 \mathrm{d}v \int_{\bar{x}(v)}^{1} \mathrm{d}x \; f\left(x,v\right) \; \frac{1}{(1-x)_+} \left(\frac{1}{(1-v)_+} + \frac{1}{v_+}\right) \\ &= \int_0^1 \mathrm{d}v \int_0^1 \mathrm{d}\tilde{x} \; \frac{1}{1-\tilde{x}} \left(\frac{f(x(\tilde{x},v),v)-f(1,v)-f(x(\tilde{x},1),1)+f(1,1)}{1-v} + \frac{f(x(\tilde{x},v),v)-f(1,v)-f(x(\tilde{x},0),0)+f(1,0)}{v}\right) \\ &+ \int_0^1 \mathrm{d}v \int_0^1 \mathrm{d}\tilde{x} \; \left(\frac{f(1,v)\ln(1-\bar{x}(v))-f(1,1)\ln(1-\bar{x}(1))}{1-v} + \frac{f(1,v)\ln(1-\bar{x}(v))-f(1,0)\ln(1-\bar{x}(0))}{v}\right), \end{aligned} \tag{A.3}$$

where in the last line of Eq. A.3 we have introduced the identity as $\int_0^1 \mathrm{d}\tilde{x}$. Similar relations are derived, in different variables, in Ref. [29].

## References


[1] T. Sjöstrand, S. Mrenna, and P. Skands, *PYTHIA 6.4 Physics and Manual*, *JHEP* **05** (2006) 026, [hep-ph/0603175].

[2] T. Sjöstrand and M. Bengtsson, *The Lund Monte Carlo for Jet Fragmentation and $e^+e^-$ Physics. Jetset Version 6.3: An Update*, *Comput. Phys. Commun.* **43** (1987) 367.

[3] M. Bengtsson and T. Sjöstrand, *Parton Showers in Leptoproduction Events*, *Z. Phys.* **C37** (1988) 465.

[4] E. Norrbin and T. Sjöstrand, *QCD Radiation off Heavy Particles*, *Nucl. Phys.* **B603** (2001) 297–342, [hep-ph/0010012].

[5] G. Miu and T. Sjöstrand, *W production in an Improved Parton Shower Approach*, *Phys. Lett.* **B449** (1999) 313–320, [hep-ph/9812455].

[6] G. Corcella *et. al.*, *HERWIG 6: An Event Generator for Hadron Emission Reactions With Interfering Gluons (including supersymmetric processes)*, *JHEP* **01** (2001) 010, [hep-ph/0011363].

[7] G. Corcella *et. al.*, *HERWIG 6.5 Release Note*, hep-ph/0210213.

[8] M. H. Seymour, *Photon Radiation in Final-State Parton Showering*, *Z. Phys.* **C56** (1992) 161–170.

[9] M. H. Seymour, *Matrix Element Corrections to Parton Shower Simulations of Deep Inelastic Scattering*, . Contributed to 27th International Conference on High Energy Physics (ICHEP), Glasgow, Scotland, 20-27 Jul 1994.

[10] G. Corcella and M. H. Seymour, *Matrix Element Corrections to Parton Shower Simulations of Heavy Quark Decay*, *Phys. Lett.* **B442** (1998) 417–426, [hep-ph/9809451].

[11] G. Corcella and M. H. Seymour, *Initial-State Radiation in Simulations of Vector Boson Production at Hadron Colliders*, *Nucl. Phys.* **B565** (2000) 227–244, [hep-ph/9908388].

[12] M. H. Seymour, *Matrix Element Corrections to Parton Shower Algorithms*, *Comp. Phys. Commun.* **90** (1995) 95–101, [hep-ph/9410414].

[13] M. H. Seymour, *A Simple Prescription for First-Order Corrections to Quark Scattering and Annihilation Processes*, *Nucl. Phys.* **B436** (1995) 443–460, [hep-ph/9410244].

[14] S. Gieseke, A. Ribon, M. H. Seymour, P. Stephens, and B. Webber, *Herwig++ 1.0: An Event Generator for $e^+e^-$ Annihilation*, *JHEP* **02** (2004) 005, [hep-ph/0311208].

[15] K. Hamilton and P. Richardson, *A Simulation of QCD Radiation in Top Quark Decays*, *JHEP* **02** (2007) 069, [hep-ph/0612236].

[16] S. Gieseke *et. al.*, *Herwig++ 2.0 Release Note*, hep-ph/0609306.

[17] M. Bähr *et. al.*, *Herwig++ 2.2 Release Note*, arXiv:0804.3053.

[18] S. Gieseke, P. Stephens, and B. Webber, *New Formalism for QCD Parton Showers*, *JHEP* **12** (2003) 045, [hep-ph/0310083].

[19] S. Frixione and B. R. Webber, *Matching NLO QCD Computations and Parton Shower Simulations*, *JHEP* **06** (2002) 029, [hep-ph/0204244].

[20] S. Frixione, P. Nason, and B. R. Webber, *Matching NLO QCD and Parton Showers in Heavy flavour Production*, *JHEP* **08** (2003) 007, [hep-ph/0305252].

[21] S. Frixione, E. Laenen, P. Motylinski, and B. R. Webber, *Single-top Production in MC@NLO*, *JHEP* **03** (2006) 092, [hep-ph/0512250].

[22] S. Frixione and B. R. Webber, *The MC@NLO 3.3 Event Generator*, hep-ph/0612272.

[23] S. Frixione, E. Laenen, P. Motylinski, and B. R. Webber, *Angular Correlations of Lepton Pairs from Vector Boson and Top Quark Decays in Monte Carlo Simulations*, *JHEP* **04** (2007) 081, [hep-ph/0702198].

[24] S. Frixione, E. Laenen, P. Motylinski, B. Webber, and C. D. White, *Single-top Hadroproduction in Association with a W Boson*, arXiv:0805.3067.

[25] O. Latunde-Dada, *Herwig++ Monte Carlo At Next-To-Leading Order for $e^+e^-$ annihilation and lepton pair production*, *JHEP* **11** (2007) 040, [arXiv:0708.4390].

[26] P. Nason, *A New Method for Combining NLO QCD with Shower Monte Carlo Algorithms*, *JHEP* **11** (2004) 040, [hep-ph/0409146].

[27] P. Nason and G. Ridolfi, *A Positive-Weight Next-to-leading-Order Monte Carlo for Z pair Hadroproduction*, *JHEP* **08** (2006) 077, [hep-ph/0606275].

[28] S. Frixione, P. Nason, and G. Ridolfi, *The POWHEG-hvq Manual Version 1.0*, arXiv:0707.3081.

[29] S. Frixione, P. Nason, and C. Oleari, *Matching NLO QCD Computations with Parton Shower Simulations: the POWHEG Method*, *JHEP* **11** (2007) 070, [arXiv:0709.2092].

[30] S. Frixione, P. Nason, and G. Ridolfi, *A Positive-Weight Next-to-Leading-Order Monte Carlo for Heavy Flavour Hadroproduction*, *JHEP* **09** (2007) 126, [arXiv:0707.3088].

[31] O. Latunde-Dada, S. Gieseke, and B. Webber, *A Positive-Weight Next-to-Leading-Order Monte Carlo for $e^+e^-$ Annihilation to Hadrons*, *JHEP* **02** (2007) 051, [hep-ph/0612281].

[32] S. Catani, F. Krauss, R. Kuhn, and B. R. Webber, *QCD Matrix Elements + Parton Showers*, *JHEP* **11** (2001) 063, [hep-ph/0109231].

[33] F. Krauss, *Matrix Elements and Parton Showers in Hadronic Interactions*, *JHEP* **08** (2002) 015, [hep-ph/0205283].

[34] A. Schälicke and F. Krauss, *Implementing the ME+PS Merging Algorithm*, *JHEP* **07** (2005) 018, [hep-ph/0503281].

[35] L. Lönnblad, *Correcting the Colour-Dipole Cascade Model with Fixed Order Matrix Elements*, *JHEP* **05** (2002) 046, [hep-ph/0112284].

[36] M. L. Mangano, M. Moretti, and R. Pittau, *Multijet Matrix Elements and Shower Evolution in Hadronic Collisions: $Wb\bar{b}+(n)$ jets as a Case Study*, *Nucl. Phys.* **B632** (2002) 343–362, [hep-ph/0108069].

[37] S. Mrenna and P. Richardson, *Matching Matrix Elements and Parton Showers with HERWIG and PYTHIA*, *JHEP* **05** (2004) 040, [hep-ph/0312274].

[38] J. Alwall *et. al.*, *Comparative Study of Various Algorithms for the Merging of Parton Showers and Matrix Elements in Hadronic Collisions*, *Eur. Phys. J.* **C53** (2008) 473–500, [arXiv:0706.2569].

[39] M. Bähr *et. al.*, *Herwig++ Physics and Manual*, arXiv:0803.0883.

[40] G. Altarelli, R. K. Ellis, and G. Martinelli, *Leptoproduction and Drell-Yan Processes Beyond the Leading Approximation in Chromodynamics*, *Nucl. Phys.* **B143** (1978) 521.

[41] J. Kubar-Andre and F. E. Paige, *Gluon Corrections to the Drell-Yan Model*, *Phys. Rev.* **D19** (1979) 221.

[42] R. Kleiss, *From Two to Three Jets in heavy Boson Decays: an Algorithmic Approach*, *Phys. Lett.* **B180** (1986) 400.

[43] L. Lönnblad, *ThePEG, PYTHIA7, Herwig++ and ARIADNE*, *Nucl. Instrum. Meth.* **A559** (2006) 246–248.

[44] G. P. Lepage, *VEGAS: An Adaptive Multidimensional Integration Program*, . CLNS-80/447.

[45] J. M. Campbell and R. K. Ellis, *Radiative Corrections to $Zb\bar{b}$ production*, *Phys. Rev.* **D62** (2000) 114012, [hep-ph/0006304].

[46] A. D. Martin, R. G. Roberts, W. J. Stirling, and R. S. Thorne, *NNLO Global Parton Analysis*, *Phys. Lett.* **B531** (2002) 216–224, [hep-ph/0201127].

[47] M. R. Whalley, D. Bourilkov, and R. C. Group, *The Les Houches Accord PDFs (LHAPDF) and Lhaglue*, hep-ph/0508110.

[48] **D0** Collaboration, V. M. Abazov *et. al.*, *Measurement of the Shape of the Boson Rapidity Distribution for $p\bar{p} \to Z/\gamma^* \to e^+e^- + X$ events produced at $\sqrt{s}$ of 1.96-TeV*, *Phys. Rev.* **D76** (2007) 012003, [hep-ex/0702025].

[49] **CDF** Collaboration, A. A. Affolder *et. al.*, *The Transverse Momentum and Total Cross Section of $e^+e^-$ pairs in the Z boson region from $p\bar{p}$ collisions at $\sqrt{s} = 1.8$ TeV*, *Phys. Rev. Lett.* **84** (2000) 845–850, [hep-ex/0001021].

[50] **D0** Collaboration, V. M. Abazov *et. al.*, *Measurement of the Shape of the Boson Transverse Momentum Distribution in $p\bar{p} \to Z/\gamma^* \to e^+e^- + X$ Events Produced at $\sqrt{s} = 1.96$ TeV*, *Phys. Rev. Lett.* **100** (2008) 102002, [arXiv:0712.0803].

[51] **D0** Collaboration, B. Abbott *et. al.*, *Measurement of the Shape of the Transverse Momentum Distribution of W bosons Produced in $p\bar{p}$ Collisions at $\sqrt{s} = 1.8$ TeV*, *Phys. Rev. Lett.* **80** (1998) 5498–5503, [hep-ex/9803003].

[52] E. L. Nurse, *A Measurement of the Inclusive $Z/\gamma^* \to \mu^+\mu^-$ Cross Section and Study of W and Z events in $p\bar{p}$ collisions at D0*, . FERMILAB-THESIS-2005-05.

[53] A. D. Martin, R. G. Roberts, W. J. Stirling, and R. S. Thorne, *Uncertainties of Predictions from Parton Distributions. I: Experimental errors*, *Eur. Phys. J.* **C28** (2003) 455–473, [hep-ph/0211080].

[54] S. Alioli, P. Nason, C. Oleari, and E. Re, *NLO vector-boson production matched with shower in POWHEG*, arXiv:0805.4802.